Engineering Innovations
ISSN: 2813-1002, Vol. 3, pp 1-12
doi:10.4028/p-d6t7o5

Submitted: 2021-09-30
Revised: 2022-03-26
Accepted: 2022-03-31
Online: 2022-09-01

MHD Slip Flow and Heat Transfer with Ohmic Heating between a Rotating Solid Disk and Stationary Permeable Disk

Sreedhara Rao Gunakala[1,a], Victor Job[2,b*] and Maraika Alexander[3,c]

[1,3]Department of Mathematics and Statistics, The University of the West Indies, St. Augustine, Trinidad and Tobago

[2]Department of Mathematics, The University of the West Indies, Mona, Jamaica

[a]sreedhara.rao@sta.uwi.edu, [b*]victor.job@uwimona.edu.jm, [c]lisamaraika@yahoo.com.

Keywords: Fluid slip, Heat transfer, MHD, Ohmic heating, Porous media, Von Karman transformations.

Abstract. In this paper, the axially-symmetric MHD (magnetohydrodynamic) slip fluid flow and heat transfer between a rotating disk and a stationary permeable disk has been examined. The physical system is comprised of a free-fluid region with an underlying fluid-saturated porous bed with a solid base. The fluid flow within the free-fluid region is modeled using the Navier-Stokes equation, whereas the flow within the porous bed is described using the Brinkman equation. The governing equations of fluid flow and heat transfer, along with the associated boundary conditions, are reduced to a system of ordinary differential equations using suitable similarity transformations. A series expansion technique is then employed in order to obtain analytical approximations for the velocity and temperature distributions. The results produced in this study are presented in graphical form. Unless otherwise stated, the following non-dimensional values are used for the numerical calculations: Hartmann number $M = 1$, Reynolds number $R = 0.1$, Darcy parameter $\beta = 0.05$, thermal conductivity ratio $\lambda = 0.5$, Eckert number $Ec = 10$, slip parameter $N^* = 0.05$, $\eta = 1$, and Prandtl numbers $Pr_1 = Pr_2 = 10$. The influence of the Darcy parameter, Hartmann number and thermal conductivity ratio on the flow velocity and fluid temperature are investigated.

Introduction

The study of fluid flows with heat transfer is of tremendous importance in engineering and the physical sciences. An important physical phenomenon that has long since become a vital part of hydrodynamics is the flow of fluid between rotating disks. Applications of this type of fluid flow can be found in the fields of biomedical engineering, chemical engineering and geophysics. In particular, the study of flows through porous media between rotating disks is useful for understanding the extraction of fluid from porous ground, the underground flow of crude oil, industrial filtration processes and the lubrication of porous bearings [1, 2].

Porous media flows between rotating and stationary disks are commonly described using either Darcy's equation or the Brinkman equation. Ehrhardt [3] explored coupling conditions at the interface between a free-flowing fluid and a fluid-saturated porous medium. The author noted that the use of the Navier-Stokes equations for the free-flow and Darcy's Law for the flow through the porous medium is inherently difficult, since the structures of the corresponding differential equations are fundamentally different. Neale and Nader [4] wrote about the relative advantage of Brinkman's law over Darcy's law, and mentioned that the lack of a macroscopic shear term in Darcy's model made it incompatible with the existence of a boundary layer region in the porous medium.

Saxena and Kumar [5] considered the MHD flow of fluid bounded by rotating disks. The Brinkman model was used to describe the flow of viscous fluid through the porous region. Hamza [1] studied the influence of uniform suction on MHD porous media flow due to an infinite permeable rotating disk. The flow domain is comprised of a free fluid region and a porous (Brinkman) region. Similarity transformations were used to reduce the governing equations to a set of nonlinear ordinary differential equations, which were solved using a series approximation technique. Gunakala et al. [6]

used the Brinkman model to investigate the heat transfer and flow of two immiscible fluids through a channel with porous beds, and the governing equations were solved using the finite element method.

The influence of radiation on the flow of fluid through a porous medium over a permeable rotating disk with velocity slip was studied by Jain and Bohra [7]. The Brinkman model was used to describe the flow through the porous medium, and temperature-dependent fluid properties were considered. Hayat et al. [8] used the Darcy-Brinkman-Forchheimer model to investigate the steady three-dimensional slip flow of nanofluid through a porous region located above a rotating disk. The governing equations for velocity, temperature and concentration were solved using the Optimal Homotopy Analysis Method, and the effects of viscous dissipation, Brownian motion and thermophoresis were examined. Gul et al. [9] considered the melting of a material and unsteady flow of the melted liquid over a permeable rotating disk under the influence of a uniform transverse magnetic field. The governing Brinkman and energy equations were solved using the homotopy analysis method, and the influence of relevant dimensionless parameters was investigated.

Sibanda and Makinde [10] conducted a numerical study on the steady MHD flow and heat transfer in a porous medium that is bounded by a rotating disk. In their study, the influence of Ohmic heating, viscous dissipation and Hall currents were considered. Jogie and Bhatt [11] explored the flow and heat transfer of a viscous incompressible fluid between a rotating solid disk and a stationary fluid-saturated naturally permeable disk. The flow was separated into 3 regions; a free-flow region, a Brinkman region and a Darcy region. In their study, the Beavers-Joseph condition was used to model the tangential slip between the Brinkman and Darcy regions. The governing differential equations were solved using a series expansion method and the shooting method. The results were presented using velocity profiles, streamlines and temperature profiles.

To the best of the authors' knowledge, the combined effects of fluid slip and Ohmic heating on the two-layer flow of fluid between two disks in the presence of an applied magnetic field have not been investigated in the existing literature. Therefore in the present work, the novel problem of a two-layer MHD slip flow and heat transfer with Ohmic heating between a rotating solid disk and a stationary permeable disk with a solid base is considered. The flow within the free-fluid region is governed by the Navier-Stokes equation and the flow within the porous region is described using the Brinkman model. A series expansion method is used to obtain approximations for the flow velocities and fluid temperature in each region. The effects of Hartmann number, Darcy parameter, slip parameter and thermal conductivity ratio on the velocity and temperature profiles in the free-fluid region (located below the rotating disk) and the underlying Brinkman region are examined in the absence and presence of an applied magnetic field.

Mathematical Model

The steady axially-symmetric flow of a laminar and incompressible Newtonian fluid between a rotating solid disk and a stationary fluid-saturated porous disk is investigated, where the vertical distance h between the disks is equal to the thickness of the porous disk as shown in Figure 1. The rotating solid disk is located at $z = h$, and has angular velocity Ω and constant temperature T_u. The stationary permeable disk has a solid base that is located at $z = -h$ and has constant temperature T_l (where $T_l \neq T_u$). A uniform magnetic field with strength B_0 is applied to the system so that the Lorentz force induced by this magnetic field acts in the radial and angular directions. The transfer of heat between the rotating disk and the stationary disk is considered along with Ohmic heating. The Navier-slip condition on the rotating disk and the no-slip condition on the solid base is considered, and it is assumed that the velocity, temperature, shear stress and heat flux are continuous at the interface between the free-flow and porous regions.

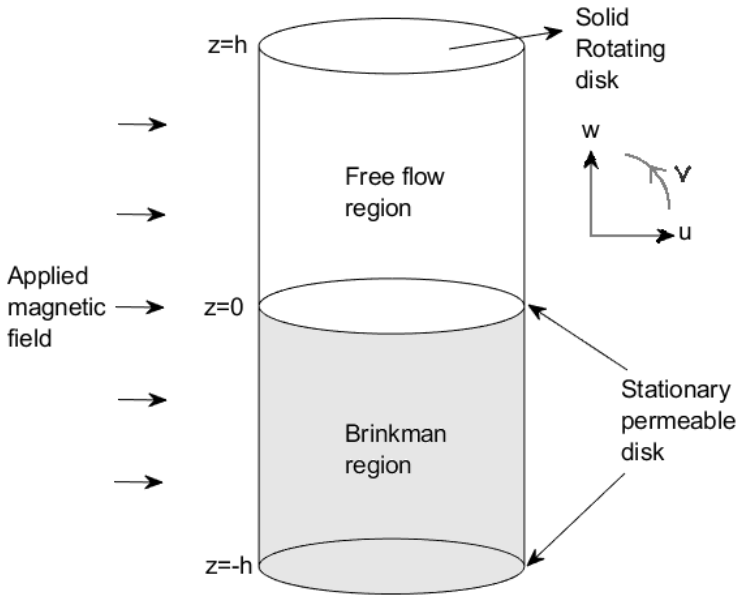

Figure 1: Schematic Diagram

Assuming that external forces on the fluid and the effects of thermal radiation and viscous dissipation are negligible, the governing equations for the problem are given below [11-13].

Zone I (Free-fluid region, $0 \le z \le h$):

Continuity Equation:

$$\frac{\partial u}{\partial r} + \frac{u}{r} + \frac{\partial w}{\partial z} = 0. \tag{1}$$

Momentum Equations:

$$\rho\left(u\frac{\partial u}{\partial r} + w\frac{\partial u}{\partial z} - \frac{v^2}{r}\right) = -\frac{\partial p}{\partial r} + \mu\left(\frac{\partial^2 u}{\partial r^2} + \frac{1}{r}\frac{\partial u}{\partial r} + \frac{\partial^2 u}{\partial z^2} - \frac{u}{r^2}\right) - \sigma B_0^2 u. \tag{2}$$

$$\rho\left(u\frac{\partial v}{\partial r} + w\frac{\partial v}{\partial z} + \frac{uv}{r}\right) = \mu\left(\frac{\partial^2 v}{\partial r^2} + \frac{1}{r}\frac{\partial v}{\partial r} + \frac{\partial^2 v}{\partial z^2} - \frac{v}{r^2}\right) - \sigma B_0^2 v. \tag{3}$$

$$\rho\left(u\frac{\partial w}{\partial r} + w\frac{\partial w}{\partial z}\right) = -\frac{\partial p}{\partial z} + \mu\left(\frac{\partial^2 w}{\partial r^2} + \frac{1}{r}\frac{\partial w}{\partial r} + \frac{\partial^2 w}{\partial z^2}\right). \tag{4}$$

Energy Equation:

$$\boldsymbol{\rho c\left(u\frac{\partial T}{\partial r} + w\frac{\partial T}{\partial z}\right) = k_1\left(\frac{\partial^2 T}{\partial r^2} + \frac{1}{r}\frac{\partial T}{\partial r} + \frac{\partial^2 T}{\partial z^2}\right) + \sigma B_0^2(u^2 + v^2)}. \tag{5}$$

Zone II (Brinkman region, $-h \le z \le 0$):

Continuity Equation:

$$\frac{\partial u_b}{\partial r} + \frac{u_b}{r} + \frac{\partial w_b}{\partial z} = 0. \tag{6}$$

Momentum Equations:

$$-\frac{\partial p_b}{\partial r} + \mu\left(\frac{\partial^2 u_b}{\partial r^2} + \frac{1}{r}\frac{\partial u_b}{\partial r} + \frac{\partial^2 u_b}{\partial z^2} - \frac{u_b}{r^2} - \frac{u_b}{k^*}\right) - \sigma B_0^2 u_b = 0. \tag{7}$$

$$\mu\left(\frac{\partial^2 v_b}{\partial r^2}+\frac{1}{r}\frac{\partial v_b}{\partial r}+\frac{\partial^2 v_b}{\partial z^2}-\frac{v_b}{r^2}-\frac{v_b}{k^*}\right)-\sigma B_0^2 v_b=0. \tag{8}$$

$$-\frac{\partial p_b}{\partial z}+\mu\left(\frac{\partial^2 w_b}{\partial r^2}+\frac{1}{r}\frac{\partial w_b}{\partial r}+\frac{\partial^2 w_b}{\partial z^2}-\frac{w_b}{k^*}\right)=0. \tag{9}$$

Energy Equation:

$$\rho c\left(u_b\frac{\partial T_b}{\partial r}+w_b\frac{\partial T_b}{\partial z}\right)=k_2\left(\frac{\partial^2 T_b}{\partial r^2}+\frac{1}{r}\frac{\partial T_b}{\partial r}+\frac{\partial^2 T_b}{\partial z^2}\right)+\sigma B_0^2(u_b^2+v_b^2)+\frac{\mu}{k^*}(u_b^2+v_b^2+w_b^2). \tag{10}$$

where r and z are the radial and axial coordinates; u, v and w are the radial, angular and axial velocity components in the free-fluid region; u_b, v_b and w_b are the radial, angular and axial velocity components in the Brinkman region; p, T and k_1 are the pressure, temperature and thermal conductivity in the free-fluid region; and p_b, T_b, k_2 and k^* are the pressure, temperature, thermal conductivity and permeability in the Brinkman region. The fluid density, viscosity, fluid specific heat capacity, electrical conductivity and the magnetic flux density are denoted by ρ, μ, c, σ and B_0 respectively. The associated boundary conditions are:

$$u=N\frac{\partial u}{\partial z},\ v=r\Omega+N\frac{\partial v}{\partial z},\ w=0 \text{ and } T=T_u \text{ when } z=h. \tag{11}$$

$$u=u_b,=v_b,w=w_b,\frac{\partial w}{\partial r}+\frac{\partial u}{\partial z}=\frac{\partial w_b}{\partial r}+\frac{\partial u_b}{\partial z},\frac{\partial v}{\partial z}=\frac{\partial v_b}{\partial z},$$
$$T=T_b \text{ and } k_1\frac{\partial T}{\partial z}=k_2\frac{\partial T_b}{\partial z} \text{ at } z=0. \tag{12}$$

$$u_b=v_b=w_b=0 \text{ and } T=T_l \text{ at } z=-h. \tag{13}$$

where N^* is the Navier slip parameter.

Method of Solution

Let $\xi=\frac{z}{h}$ and $\eta=\frac{r}{h}$ be the non-dimensional axial and radial coordinates respectively, and consider the Von Karman transformations

$$u=r\Omega F(\xi),\ v=r\Omega G(\xi),\ w=\sqrt{\frac{\mu\Omega}{\rho}}H(\xi),\ u_b=r\Omega F_b(\xi),\ v_b=r\Omega G_b(\xi),$$
$$w_b=\sqrt{\frac{\mu\Omega}{\rho}}H_b(\xi),\ p=\mu\Omega P^*(\xi)+\frac{\rho}{2}K\Omega^2 r^2,\ T=[T_u-T_l]\theta(\xi)+T_l,$$
$$p_b=\mu\Omega P_b^*(\xi)+\frac{\rho}{2}K\Omega^2 r^2,\ T_b=[T_u-T_l]\theta_b(\xi)+T_l. \tag{14}$$

Approximations for the velocity and temperature within the free-fluid and Brinkman regions are obtained by taking the following series expansions [15] for low Reynolds number:

$$F(\xi)=RF_1(\xi)+R^3F_2(\xi)+O(R^5),\qquad F_b(\xi)=RF_{1b}(\xi)+R^3F_{2b}(\xi)+O(R^5). \tag{15}$$

$$G(\xi)=G_1(\xi)+R^2G_2(\xi)+O(R^4),\qquad G_b(\xi)=G_{1b}(\xi)+R^2G_{2b}(\xi)+O(R^4). \tag{16}$$

$$H(\xi)=R^{3/2}H_1(\xi)+R^{7/2}H_2(\xi)+O\left(R^{11/2}\right),$$
$$H_b(\xi)=R^{3/2}H_{1b}(\xi)+R^{7/2}H_{2b}(\xi)+O\left(R^{11/2}\right) \tag{17}$$
$$\theta(\xi)=\theta_1(\xi)+R^2\theta_2(\xi)+O(R^4),\qquad \theta_b(\xi)=\theta_{1b}(\xi)+R^2\theta_{2b}(\xi)+O(R^4). \tag{18}$$

$$K=K_1+R^2K_2+O(R^4) \tag{19}$$

Substituting these series expansions and comparing the coefficients of the lowest powers of R, the equations below are obtained.

First Set of Equations:

$$F_1'' - M^2 F_1 = K_1 - G_1^2,\ G_1'' - M^2 G_1 = 0,\ H_1' = -2F_1,\ \theta_1'' + \eta^2 M^2 Pr_1 Ec G_1^2 = 0 \tag{20}$$

$$F_{1b}'' - \left(M^2 + \frac{1}{\beta}\right) F_{1b} = K_1,\ G_{1b}'' - \left(M^2 + \frac{1}{\beta}\right) G_{1b} = 0,\ H_{1b}' = -2F_{1b},$$
$$\theta_{1b}'' + \eta^2 Pr_1 Ec \left(M^2 + \frac{1}{\beta}\right) G_{1b}^2 = 0 \tag{21}$$

Second Set of Equations:

$$F_2'' - M^2 F_2 = H_1 F_1' + F_1^2 - 2G_1 G_2 + K_2,\ G_2'' - M^2 G_2 = 2F_1 G_1 + H_1 G_1',$$
$$H_2' = -2F_2,\ \theta_2'' - Pr_2 H_1 \theta_1' + \eta^2 M^2 Pr_2 Ec (F_1^2 + G_1 G_2) = 0 \tag{22}$$

$$F_{2b}'' - \left(M^2 + \frac{1}{\beta}\right) F_{2b} = K_2,\ G_{2b}'' - \left(M^2 + \frac{1}{\beta}\right) G_{2b} = 0,\ \ H_{2b}' = -2F_{2b},$$
$$\theta_{2b}'' - Pr_2 H_{1b} \theta_{1b}' + \eta^2 Pr_2 Ec \left[\left(M^2 + \frac{1}{\beta}\right)(F_{1b}^2 + G_{1b} G_{2b}) + \frac{H_{1b}^2}{\eta^2}\right] = 0. \tag{23}$$

The associated boundary conditions are

$$F_n(1) = N^* F_n'(1),\ H_n(1) = 0 \text{ for } n = 1,2,$$
$$G_1(1) - N^* G_1'(1) = \theta_1(1) = 1 \text{ and } G_2(1) - N^* G_2'(1) = \theta_2(1) = 0 \tag{24}$$

$$F_n(0) = F_{nb}(0),\ F_n'(0) = F_{nb}'(0),\ G_n(0) = G_{nb}(0),\ G_n'(0) = G_{nb}'(0),\ H_n(0) = H_{nb}(0),$$
$$\theta_n(0) = \theta_{nb}(0) \text{ and } \theta_n'(0) = \lambda \theta_{nb}'(0) \text{ for } n = 1,2 \tag{25}$$

$$F_{nb}(-1) = G_{nb}(-1) = H_{nb}(-1) = \theta_{nb}(-1) = 0 \text{ for } n = 1,2 \tag{26}$$

In order to visualize the fluid flow within the free-fluid and Brinkman regions, the stream functions ψ and ψ_b [14] are considered as defined by

$$\psi = \eta^2 H(\xi) \text{ and } \psi_b = \eta^2 H_b(\xi) \tag{27}$$

with boundary conditions

$$\psi = 0 \text{ at } \xi = 1;\ \psi = \psi_b \text{ at } \xi = 0; \text{ and } \psi_b = 0 \text{ at } \xi = -1. \tag{28}$$

The equations and corresponding boundary conditions obtained in (20)-(28) are solved analytically using the mathematical software Maple, and then the results obtained from this analytical solution are presented graphically using the mathematical software MATLAB.

Discussion of Results

Numerical results are obtained from the analytical approximations and presented as graphical plots of velocity and temperature for different values of the Darcy parameter, Hartmann number, thermal conductivity ratio and slip parameter. Unless otherwise stated, the following non-dimensional values are used for the numerical calculations: $M = 1$, $R = 0.1$, $\beta = 0.05$, $\lambda = 0.5$, $Ec = 10$, $N^* = 0.05$, $\eta = 1$, $Pr_1 = Pr_2 = 10$. For ease of notation in the graphical plots, the radial, angular and axial flow velocity components, the fluid temperature and the stream function are denoted by F, G, H, T and ψ (respectively) in the free-fluid and Brinkman regions.

Figures 2 to 5 display the velocity components F, H, G and temperature θ for different values of the Darcy parameter β. From figures 2 to 4, it is seen that when β increases, the magnitude of the

velocity components F, H and G are increased in both free-fluid and Brinkman regions; this is caused by an increase in the permeability of the Brinkman region and a corresponding increase in flow resistance within the porous medium. The frictional heating generated by this increased flow resistance within the Brinkman region causes the fluid temperature to increase (Figure 5) when β is increased.

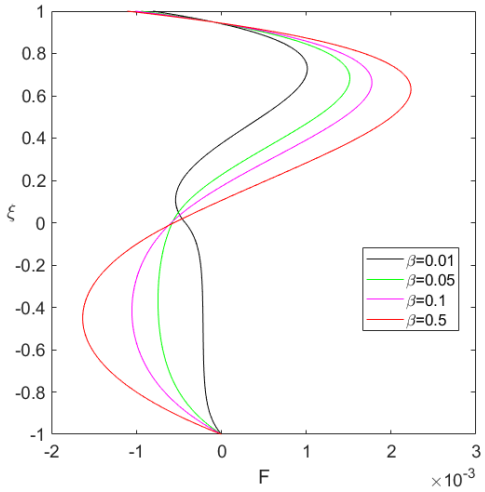

Figure 2: Plot of ξ vs F for different values of β

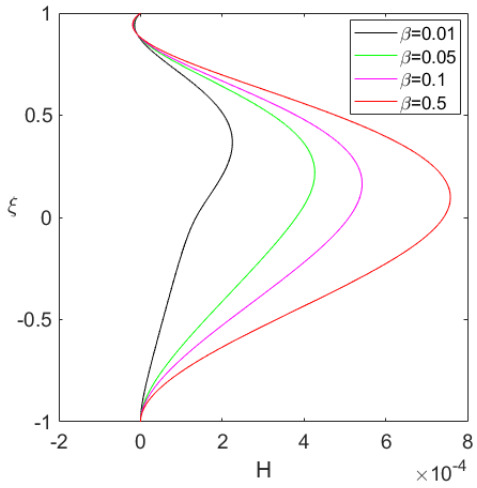

Figure 3: Plot of ξ vs H for different values of β

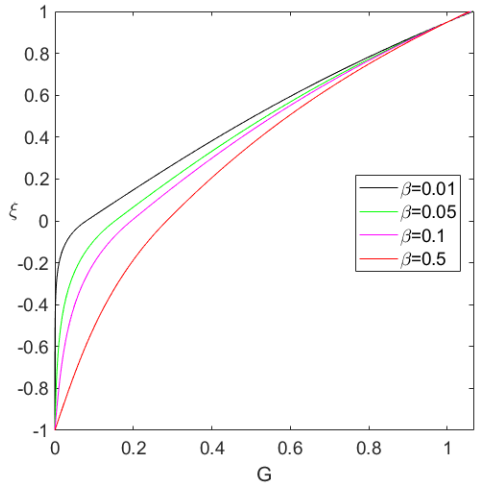

Figure 4: Plot of ξ vs G for different values of β

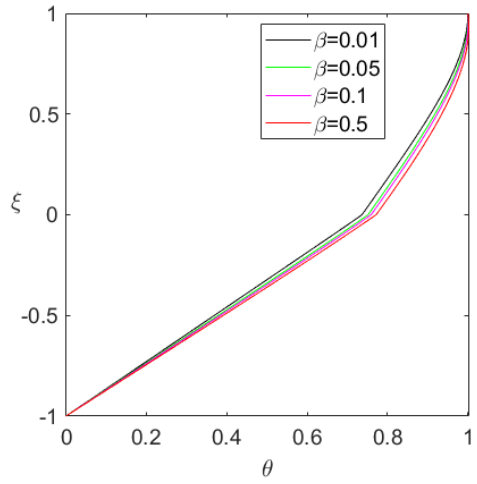

Figure 5: Plot of ξ vs θ for different values of β

Figures 6 to 9 illustrate the impact of varying the Hartmann number M on the velocity components F, H, G and temperature θ. The results indicate that the plots for F, H and G, for relatively small values of M, are similar in pattern to the ones obtained without the MHD influence. It is also noticed that in the absence of a magnetic field ($M = 0$), the radial and axial velocity profiles (Figure 6 and 7) are approximately parabolic with the maximum magnitude occurring within the free-fluid region (near the upper disk); this is consistent with the work of Krishna, Rao, and Murthy [16]. However, the values of each velocity component attained with non-zero values of M is lower than that obtained with $M = 0$. This is due to a resistive force which (as per Faraday's Second Law) is produced by the conducting fluid moving through a magnetic field. This effective drag on the fluid, is larger for stronger magnetic fields [13] (reflected by larger values of Hartmann number M). Consequently, the flow velocity decreases as M increases. Indeed, the plot for each component (F, H and G), for a relatively large value of M (for example $M = 3$), suggests that the drag force produced is large enough to significantly alter or distort the flow patterns obtained for relatively small values of M. The

large drag force is further enhanced by other resistive forces being induced by fluid particles moving outwards or upwards, as described earlier. These forces could account for the relative shift of the maximum value of the curves for $M = 3$. It is observed in Figure 8 that increasing the value of M causes an increase in the angular velocity slip on the rotating disk; this is due to an increase in the angular velocity gradient near the disk as the strength of the magnetic field increases. Moreover, the temperature in the free-fluid and Brinkman regions increases with increased M (Figure 9) due to an enhancement of Ohmic heating within the fluid.

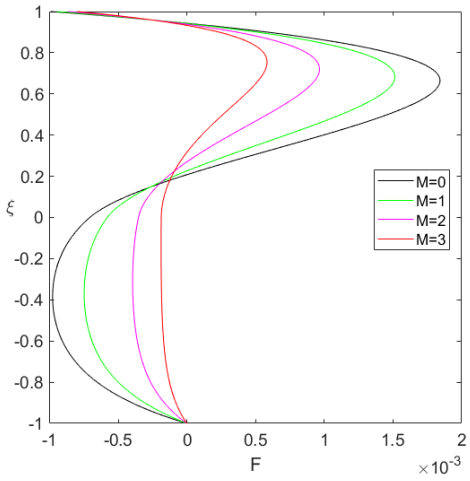

Figure 6: Plot of ξ vs F for different values of M

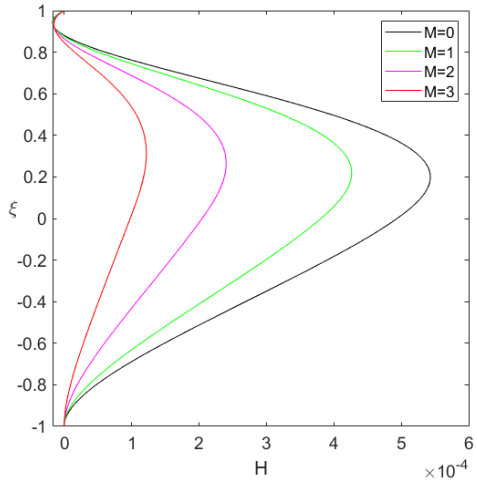

Figure 7: Plot of ξ vs H for different values of M

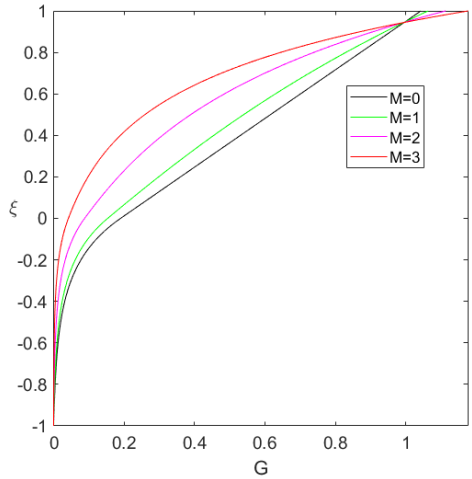

Figure 8: Plot of ξ vs G for different values of M

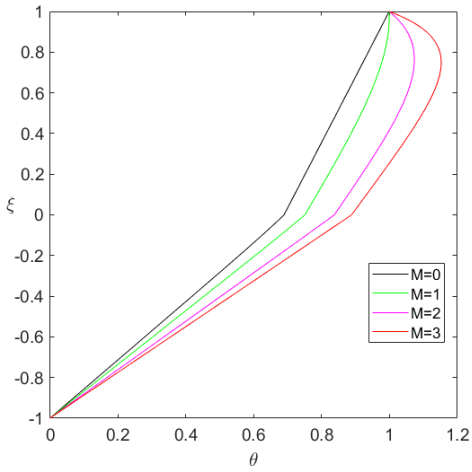

Figure 9: Plot of ξ vs θ for different values of M

The influence of the slip parameter N^* on the velocity components F, H, G and temperature θ are displayed in Figures 10 to 13. These figures show that each of the velocity components is reduced when N^* increases; this is caused by a reduction in the centrifugal forces acting on the fluid as the adhesion of fluid particles on the surface of the rotating disk is decreased. It is also noticed that there is a region near the rotating disk within which a reversal of fluid flow occurs in the radial and axial directions (Figure 10 and 11); this region increases in size as N^* is increased. The temperature within the free-fluid and Brinkman regions increase with increased N^* as a result of a reduction in thermal advection.

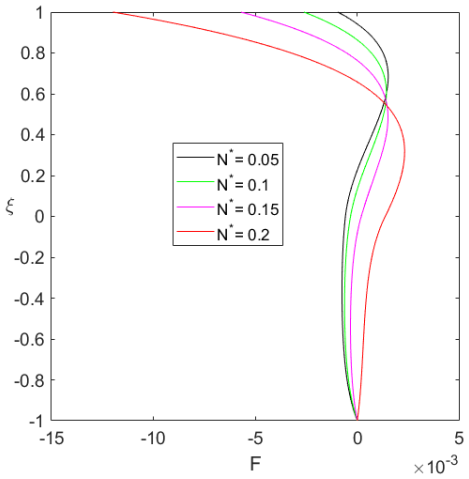

Figure 10: Plot of ξ vs F for different values of N^*

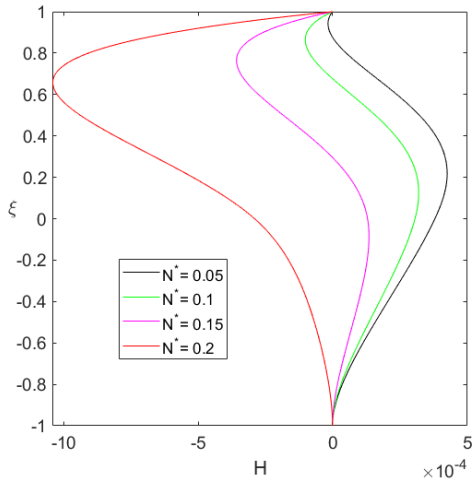

Figure 11: Plot of ξ vs H for different values of N^*

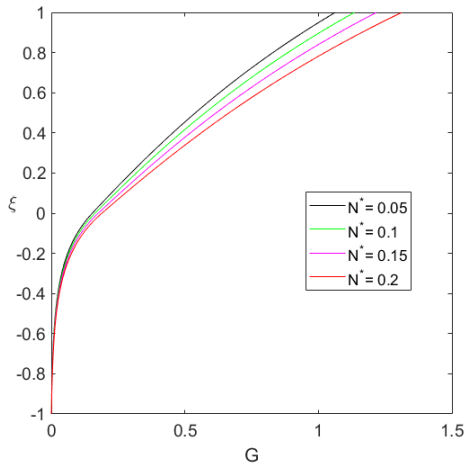

Figure 12: Plot of ξ vs G for different values of N^*

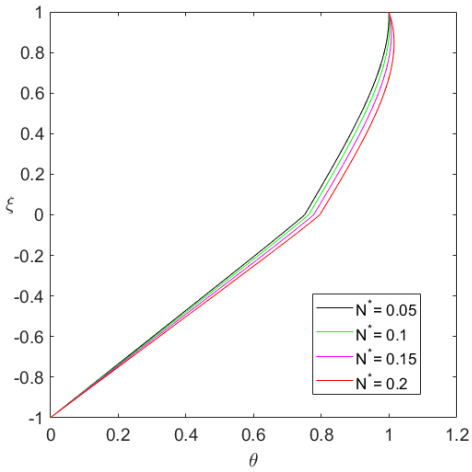

Figure 13: Plot of ξ vs θ for different values of N^*

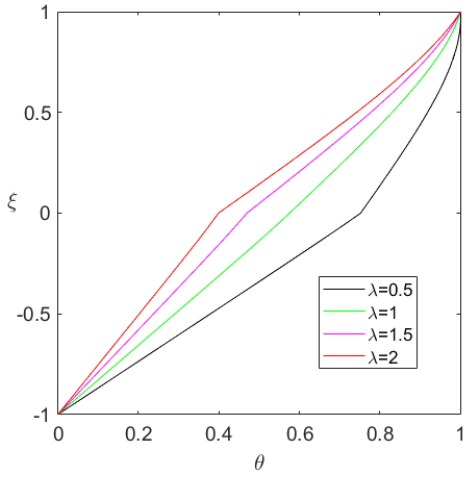

Figure 14: Plot of ξ vs G for different values of λ

Figure 14 shows the variation of fluid temperature with different values of the ratio λ of thermal conductivities in the porous and free-flow regions. The thermal conductivity ratio λ was found to have no significant impact on the velocity of the fluid; however, λ has a significant effect on the

temperature profiles. When λ is increased, the transfer of energy from the rotating solid disk to the stationary porous disk through the fluid is reduced. Consequently, as shown in Figure 18, increasing λ leads to a reduction in the temperature of the fluid.

It is observed in Figure 15 that when the value of β is increased, the spacing of the streamlines is reduced in both the free-fluid and non-porous regions; this is consistent with an increase in flow velocity in each region as β increases (see Figures 2 to 4). Furthermore, the distortion of streamlines in the porous region is reduced for increasing values of β due to a decrease in flow resistance as the permeability of the porous medium increases.

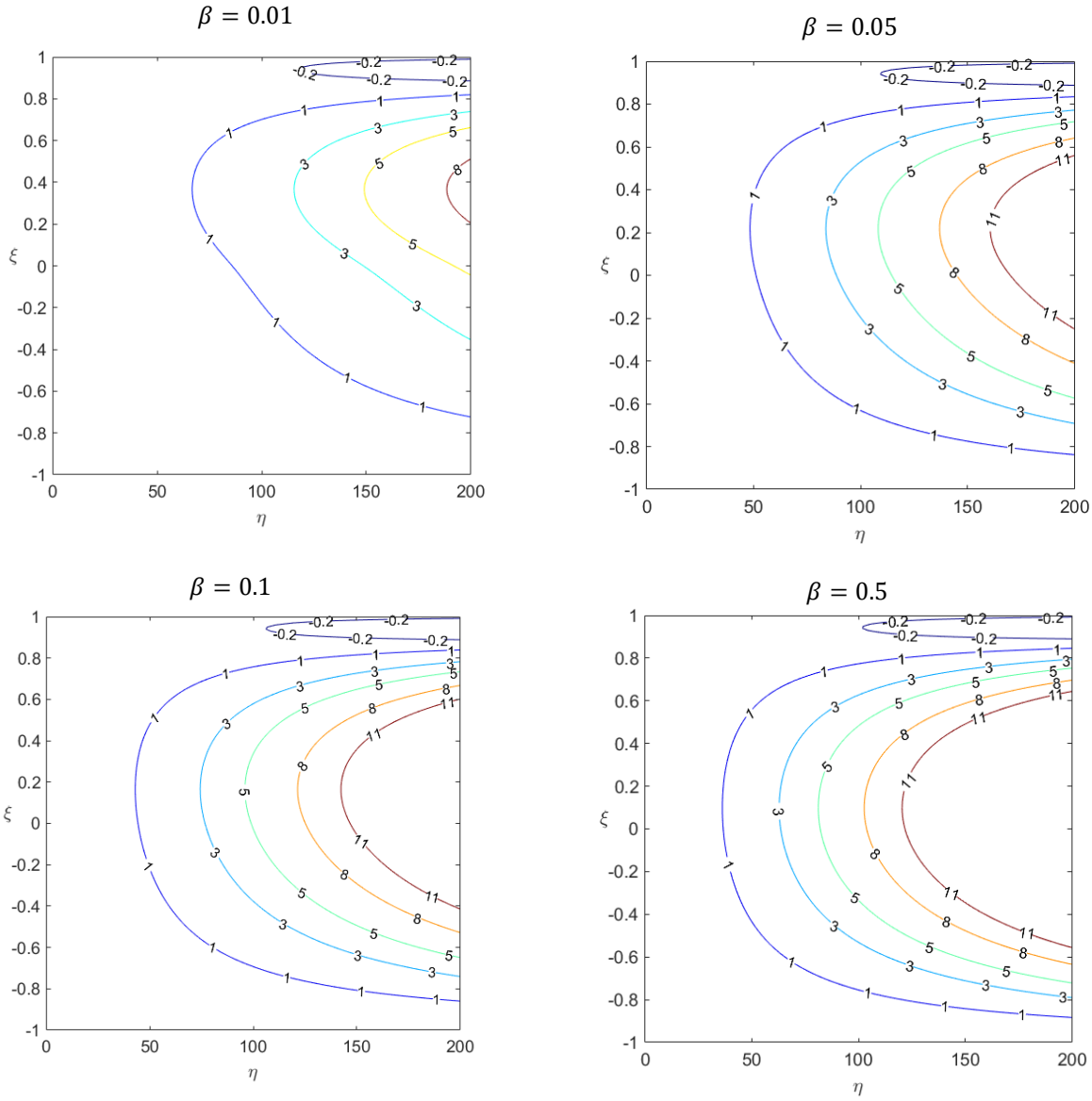

Figure 15: Streamline Plots for Different Values of β

The magnitude of the stream function within the free-fluid and Brinkman regions decreases with increased M (Figure 16) due to the suppression of fluid flow by the applied magnetic field. It is seen in Figure 17 that the values of the stream function decrease as the slip parameter N^* is increased; this is consistent with a reduction in flow velocity with increased N^* (see Figures 10 to 12). Moreover, the size of the flow reversal region increases with increased N^* until a complete flow reversal occurs in the radial and axial directions when N^* is sufficiently large ($N^* = 0.2$).

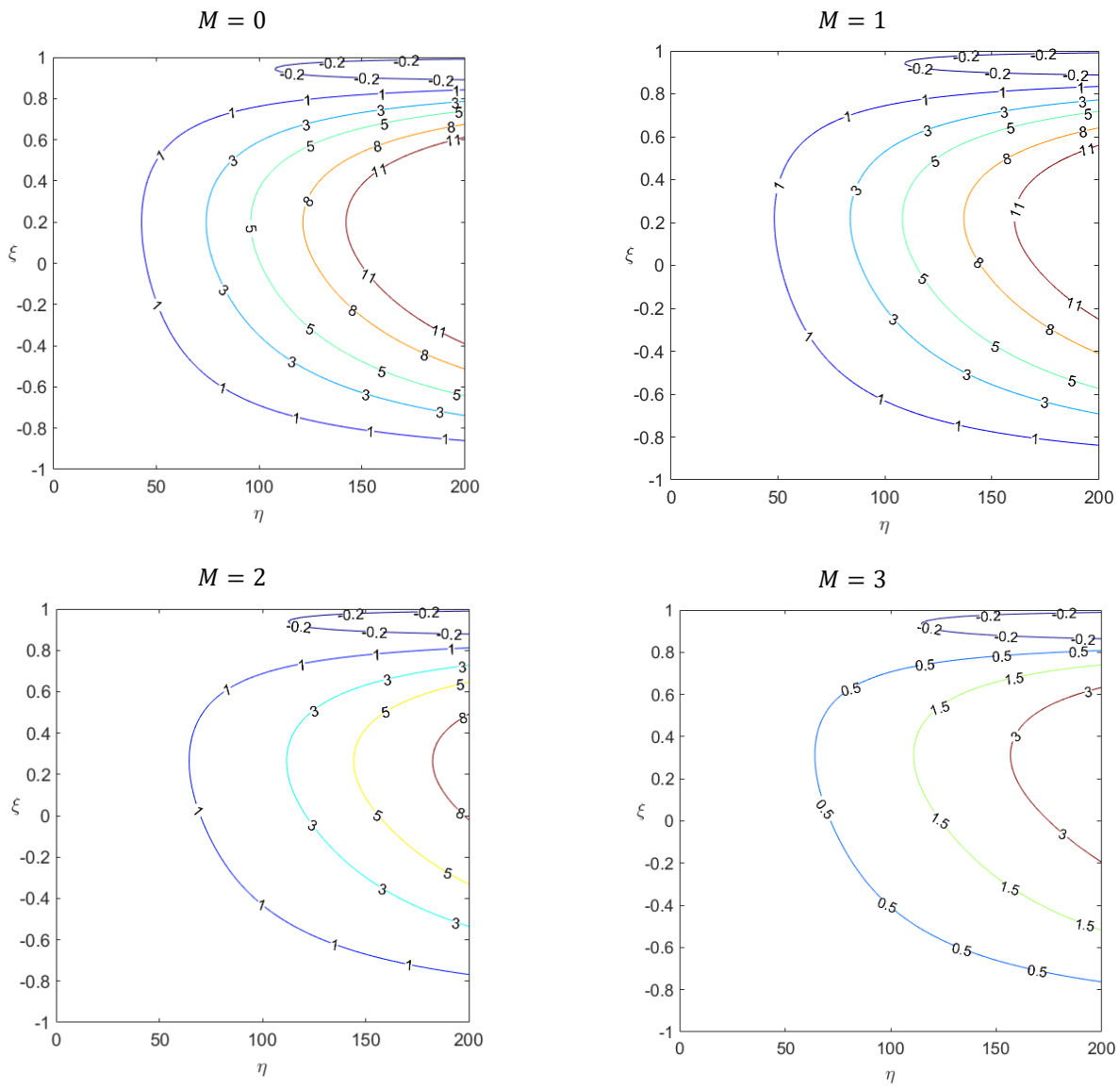

Figure 16: Streamline Plots for Different Values of M

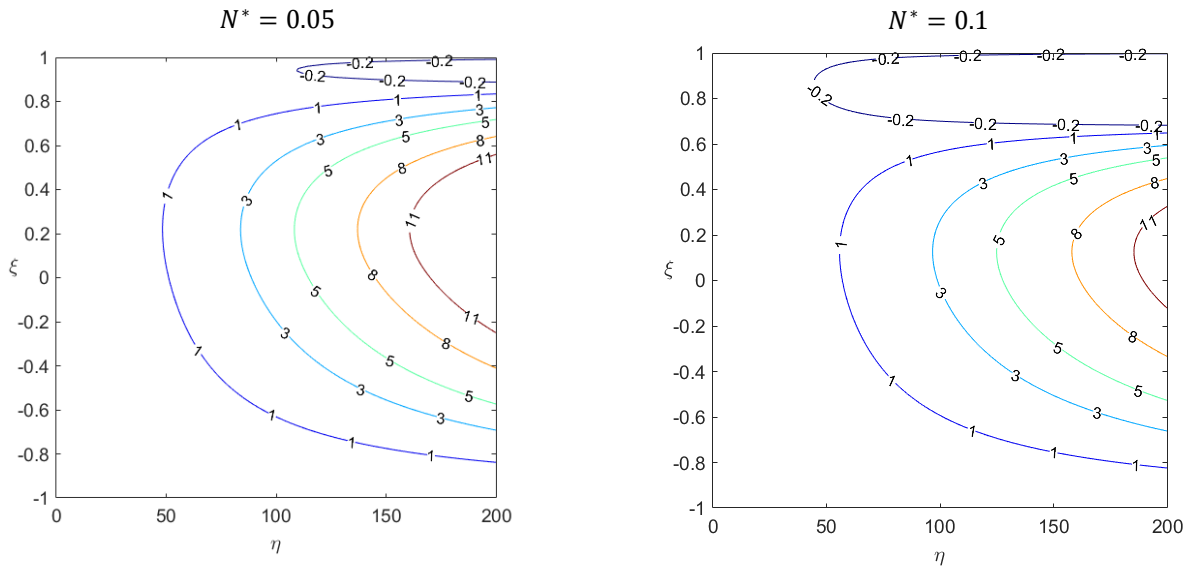

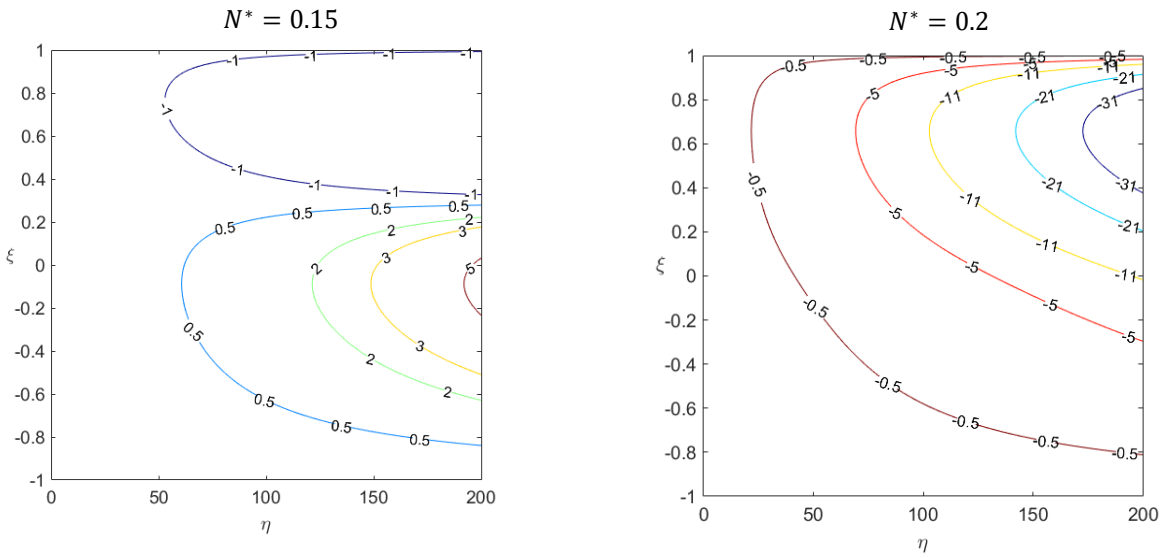

Figure 17: Streamline Plots for Different Values of N^*

Conclusions

The present work investigates the steady fluid flow and heat transfer between a rotating disk and a stationary fluid-saturated permeable disk in the presence of a transverse magnetic field. Based on the results obtained in this study, the main conclusions are as follows:

- The magnitude of the flow velocity in the free-flow and porous regions can be increased by increasing the Darcy parameter, and can be reduced by increasing the strength of the magnetic field. Furthermore, the flow velocity can be reduced by increasing fluid slip on the rotation disk.
- The temperature of the fluid in the free-flow and porous regions can be increased by increasing the Darcy parameter, Hartmann number and slip parameter, and by decreasing the thermal conductivity ratio.
- The displacement of streamlines from the vertical axis is greater as the radial coordinate η increases.
- The magnitude of the stream function can be increased by increasing the Darcy parameter and decreasing the magnetic field strength. The stream function values are decreased by increasing the fluid slip on the rotating disk

The size of the flow reversal region increases when the amount of fluid slip on the rotating disk is increased.

References

[1] S.E.E. Hamza, Effect of Uniform Suction on MHD Flow Through Porous Medium Due To A Rotating Disk, International Journal of Scientific & Engineering Research 5(12) (2014) 896-902.

[2] P. Zandbergen, D. Dijkstra, Von Kármán swirling flows, Annual Rev. Fluid. Mech. 19 (1987) 465–491.

[3] M. Ehrhardt, An introduction to fluid-porous interface coupling, Progress in computational physics 2 (2010) 3–12. doi: 10.2174/978160805254711201010003.

[4] G. Neale, W. Nader, Practical significance of Brinkman's extension of Darcy's law: coupled parallel flows within a channel and a bounding porous medium, The Canadian Journal of Chemical Engineering 52(4) (1974) 475–478. doi: https://doi.org/10.1002/cjce.5450520407.

[5] P. Saxena, L. Kumar, A study of the effect of magnetic field on the rotation of a viscous fluid near a porous medium with a constant suction, Int. J. Eng. Sci. Tech. 6 (2014) 64–76. doi: 10.4314/ijest.v6i4.6.

[6] S.R. Gunakala, B. Bhatt, D.M.G. Comissiong, D.V. Krishna, Heat Transfer in Immiscible Fluids through a Channel with Porous Beds Bounded by Differentially Heated Plates Using Galerkin's Finite Element Method, Journal of Mathematics Research 3(2) (2011) 74-97. doi: 10.5539/jmr.v3n2p74.

[7] S. Jain, S. Bohra, Radiation Effects in Flow through Porous Medium over a Rotating Disk with Variable Fluid Properties, Advances in Mathematical Physics 2016 (2016) 9671513. doi: https://doi.org/10.1155/2016/9671513.

[8] T. Hayat, F. Hayat, T. Muhammad, A. Alsaedi, Darcy-Forchheimer flow by rotating disk with partial slip, Applied Mathematics and Mechanics 41 (2020) 741-752. doi: https://doi.org/10.1007/s10483-020-2608-9.

[9] T. Gul, R.S. Gul, W. Noman, F. Hussain, I.S. Amiri, Controlling of the melting through porous medium and magnetic field, Measurement and Control 54(5-6) (2021) 779-789. doi: https://doi.org/10.1177/0020294020919918.

[10] P. Sibanda, O.D. Makinde, On steady MHD flow and heat transfer past a rotating disk in a porous medium with ohmic heating and viscous dissipation, International Journal of Numerical Methods for Heat & Fluid Flow 20(3) (2010) 269-285. doi: https://doi.org/10.1108/09615531011024039.

[11] D.C. Jogie, B. Bhatt, The study of fluid flow and heat transfer of a viscous incompressible fluid between a rotating solid disk and a stationary permeable disk using the Brinkman-Darcy model, ZAMM-Journal of Applied Mathematics and Mechanics/Zeitschrift für Angewandte Mathematik und Mechanik 96 (5) (2016) 620–632. doi: https://doi.org/10.1002/zamm.201400089.

[12] D. Nield, A. Bejan, Convection in Porous Media, third ed., New York, Springer Science+Business Media, Inc, 2006.

[13] S. Eskinazi, Vector Mechanics of Fluids and Magnetofluids, New York, Academic Press, 1967.

[14] P.D. Verma, B.S. Bhatt, On the steady flow between a rotating and a stationary naturally permeable disc, International Journal of Engineering Science 13(9-10) (1975) 869–879.

[15] G. Batchelor, Note on a class of solutions of the Navier-Stokes equations representing steady rotationally-symmetric flow, Q. J. Mech. Appl. Maths 4 (1951) 29–41.

[16] D.V. Krishna, D.R.V. Prasada Rao, A.S. Ramachandra Murthy, Hydromagnetic convection flow through a porous medium in axially varying pipe, Journal of Engineering Physics and Thermophysics 79(4) (2006) 727. doi: 10.1007/s10891-006-0158-2.